DOI: 10.18727/0722-6691/5110

Witnessing the Early Growth and Life Cycle of Galaxies with KMOS^{3D}

Natascha M. Förster Schreiber[1]
David Wilman[2,1]
Emily S. Wisnioski[1,3,4]
Matteo Fossati[1,2,5]
J. Trevor Mendel[1,2,3,4]
Ralf Bender[2,1]
Reinhard Genzel[1,6]
Alessandra Beifiori[2,1]
Sirio Belli[1]
Gabe Brammer[7]
Andreas Burkert[2,1]
Jeffrey Chan[8]
Richard I. Davies[1]
Rebecca L. Davies[1]
Maximilian Fabricius[1,2]
Audrey Galametz[1,2,9]
Rodrigo Herrera-Camus[1]
Philipp Lang[10]
Dieter Lutz[1]
Ivelina Momcheva[11]
Thorsten Naab[12]
Erica J. Nelson[1,13]
Sedona H. Price[1]
Alvio Renzini[14]
Roberto Saglia[1,2]
Stella Seitz[2]
Taro Shimizu[1]
Amiel Sternberg[15]
Linda J. Tacconi[1]
Ken-ichi Tadaki[16]
Hannah Übler[1]
Pieter G. van Dokkum[17]
Stijn Wuyts[18]

[1] Max-Planck-Institut für Extraterrestrische Physik, Garching, Germany
[2] Universitäts-Sternwarte, Ludwig-Maximilians-Universität, Munich, Germany
[3] Research School of Astronomy & Astrophysics, Australian National University, Canberra, Australia
[4] ASTRO3D – ARC Centre for Excellence in All-Sky Astrophysics in 3D, Canberra, Australia
[5] Department of Physics, Durham University, UK
[6] Department of Physics and Astronomy, University of California, Berkeley, USA
[7] Cosmic Dawn Center, Niels Bohr Institute, University of Copenhagen, Denmark
[8] Physics and Astronomy Department, University of California, Riverside, USA
[9] Geneva Observatory, University of Geneva, Switzerland
[10] Max-Planck-Institut für Astronomie, Heidelberg, Germany
[11] Space Telescope Science Institute, Baltimore, USA
[12] Max-Planck-Institut für Astrophysik, Garching, Germany
[13] Harvard-Smithsonian Center for Astrophysics, Cambridge, USA
[14] INAF–Osservatorio Astronomico di Padova, Italy
[15] School of Physics and Astronomy, Tel Aviv University, Israel
[16] National Astronomical Observatory of Japan, Mitaka, Tokyo, Japan
[17] Astronomy Department, Yale University, New Haven, USA
[18] Department of Physics, University of Bath, UK

Near-infrared integral field unit (IFU) spectrographs are powerful tools for investigating galaxy evolution. We report on our recently completed multi-year KMOS^{3D} survey of Hα, [N II] and [SII] line emission of galaxies at redshift z ~ 0.7–2.7 with the K-band Multi-Object Spectrograph (KMOS) at the Very Large Telescope (VLT). With deep observations of 745 targets spanning over two orders of magnitude in galaxy mass, five billion years of cosmic time, and all levels of star formation, KMOS^{3D} provides an unparalleled population-wide census of spatially-resolved kinematics, star formation, outflows and nebular gas conditions. The dataset sheds new light on the physical mechanisms driving the early growth and lifecycle of galaxies, and provides a rich legacy for the astronomical community.

The regulated growth of galaxies at "cosmic noon"

Extensive panchromatic look-back surveys have now mapped the global evolution of star formation and nuclear activity, stellar mass buildup, and gas content of galaxies out to redshift z ~ 3, spanning 85% of the Universe's history. At z ~ 2, 10 billion years ago, the cosmic star formation and supermassive black hole accretion rates peaked at ~ 20 times present-day levels, and cold molecular gas accounted for as much as half the baryonic mass of galaxies. At this epoch, often dubbed "cosmic noon", ~95% of star-forming galaxies (SFGs) already lie on a tight main sequence (MS), their star formation rate (SFR) being roughly proportional to their stellar mass, SFR $\propto M_*$. These early SFGs also show relationships between their stellar mass, size, gas content, and metallicity. The growth of galaxies at cosmic noon thus appears to be tightly regulated until they reach M_* ~ 10^{11} M_*, when their star formation activity is rapidly quenched.

These observations have established the broad scope of the equilibrium growth model, in which accretion from the cosmic web and minor mergers fairly continuously replenish the gas reservoirs of SFGs, and the balance between accretion, star formation, and outflows governs their evolution. Given the different conditions prevailing in early SFGs, detailed *in-situ* observations are necessary to understand which processes regulate their evolution, how the disc and spheroidal components of present-day galaxies arise, and why star formation shuts down at high masses.

The role of near-infrared integral field unit surveys and KMOS^{3D}

Spatially and spectrally resolved information on the kinematics, star formation, and condition of the interstellar medium on sub-galactic scales provides insights into the physics that drives the early evolution of galaxies. Nebular emission lines such as Hα, [N II], [S II] and [O III] are powerful tools for investigating these properties. At z ~ 1–3, these optical lines at rest are redshifted into the near-infrared (near-IR, λ ~ 1–2.5 μm) and strongly dimmed. Dissecting distant galaxies requires sensitive near-IR instrumentation and a large collecting area. Observations with the Spectrograph for INtegral Field Observations in the Near Infrared (SINFONI) at the VLT and other near-IR single-object IFUs on 8–10-metre telescopes (for example, Förster Schreiber et al., 2011; Glazebrook, 2013) yielded the first compelling evidence that the majority of massive z ~ 2 SFGs are rotating yet turbulent discs, rather than disturbed major mergers. These pioneering studies uncovered the role of galaxy-internal processes, such as violent disc instabilities, in the gas-rich SFGs at z ~ 1–2, laying some of the foundations of the equilibrium growth framework. With 24 deploya-

ble IFUs, KMOS at the VLT brought the next breakthroughs by enabling near-IR IFU surveys of much larger and more complete samples.

We have carried out KMOS^{3D}, a comprehensive 75-night Guaranteed Time Observation (GTO) survey of Hα+[N II]+[S II] emission of 745 mass-selected galaxies at $z \sim 0.7$–2.7 (Wisnioski et al., 2015). The cornerstones of the survey strategy were: 1) wide and homogeneous coverage of galaxy stellar mass, SFR, colours, and redshift; 2) the same spectral diagnostics across the entire redshift range; and 3) deep integrations to map faint, extended line emission. The targets were drawn from the Hubble Space Telescope (HST) 3D-HST Treasury Survey (for example, Momcheva et al., 2016), which provided a well characterised parent sample with source detection and accurate redshifts relying on rest-optical properties, largely reducing the bias towards blue, actively star-forming galaxies resulting from rest-ultraviolet identifications. 3D-HST overlaps with the CANDELS fields, with high-resolution HST optical and near-IR imaging, and with extensive X-ray to far-IR/radio coverage.

The KMOS^{3D} selection criteria were:
(1) $M_* > 10^9\ M_\odot$ and a magnitude cut of $K_{AB} < 23$ mag;
(2) a redshift $0.7 < z < 2.7$;
(3) the emission lines of interest falling in atmospheric windows away from bright sky lines.
By avoiding selection on colours or properties sensitive to star formation or AGN activity, and by covering five billion years of cosmic time, KMOS^{3D} is optimally suited for population censuses and evolutionary studies.

Figure 1 shows the distribution of the KMOS^{3D} sample in stellar mass versus SFR. The *K*-band magnitude cut ensures 95% completeness for $\log(M_*/M_\odot) > 9.7$ at $0.7 < z < 1.1$; $\log(M_*/M_\odot) > 10.2$ at $1.3 < z < 1.7$; and $\log(M_*/M_\odot) > 10.5$ at $1.9 < z < 2.7$ — these correspond to the redshift slices where Hα is observed in the *YJ*-, *H*-, and *K*-bands, respectively. The corresponding median on-source integration times are 5, 8, and 9 hours respectively, and range up to 20–30 hours. The median resolution is 0.5 arcseconds, or ~ 4 kpc at at $z \sim 0.7$–2.7. Down to SFRs ~ 1/7 of the MS (comprising 80% of the sample), 90% of the objects are detected in Hα and 80% of them are resolved. Unsurprisingly, the detection rate drops among more quiescent galaxies, but even ~ 25% of those are detected, and a third of them are resolved. Selected key results are highlighted here.

The prevalence of rotationally supported turbulent gas-rich discs

First and foremost, the spatially-resolved gas motions derived from the Hα emission line profile across the KMOS^{3D} galaxies robustly confirmed that the majority (> 70%) of high-redshift SFGs are rotating discs (Figure 2). The data also confirmed the elevated gas turbulence of high-redshift discs, with typical intrinsic disc velocity dispersions $\sigma_0 \sim 50$ km s^{-1} at $z \sim 2.3$ and ~ 30 km s^{-1} at $z \sim 0.9$ (Figure 3). The increase of the velocity dispersions with redshift is in line with expectations for gravity-driven turbulence in marginally stable gas discs and the cosmic evolution in gas fractions, where heating is caused by rapid gas flows onto and within the galaxies (for example, Genzel et al., 2011; Krumholz et al., 2018).

Bulge formation, outer disc kinematics, and the dominance of baryons

Dissipative processes should be particularly efficient in discs at $z \sim 1$–3 given their gas-richness and elevated turbulence. The associated inward mass transport and angular momentum loss could lead to bulge formation on Gyr timescales. Massive stellar bulges are in place, and large nuclear concentrations of molecular gas have been uncovered as early as $z \sim 2.5$ in massive star-forming discs (for example, Lang et al., 2014; Tadaki et al., 2017). Measurements of the angular momenta of KMOS^{3D} discs further support bulge formation via disc-internal mechanisms (Burkert et al., 2016). The specific angular momenta of the discs anti-correlate with their galaxy-wide stellar and gas mass surface densities, but exhibit no significant trend with stellar mass surface densities in the inner 1 kpc. Accumulation of low angular momentum material to form bulges in the disc centres thus appears to be decoupled from the mechanisms that set disc structure and angular momentum on global galactic scales.

KMOS^{3D} has strengthened the key finding from smaller samples that $z \sim 1$–2.5 SFGs are not only gas-rich but also strongly

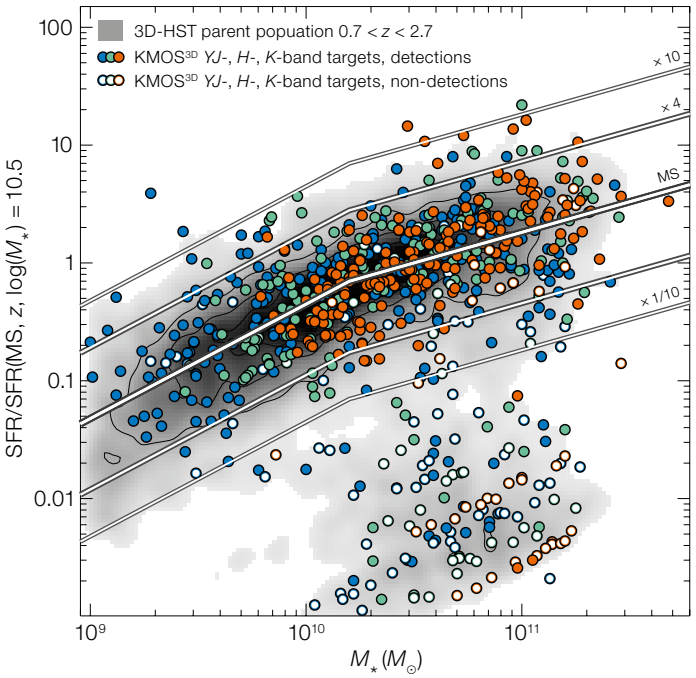

Figure 1. Distribution of the 745 KMOS^{3D} targets in stellar mass versus SFR normalised to that of the MS at the redshift of each galaxy and $\log(M_*/M_\odot) = 10.5$. The shape of the MS (from Whitaker et al., 2014) and offsets by factors of 4 and 10 above and below the relationship are plotted as solid lines. Coloured symbols represent targets observed in the *YJ*-, *H*-, and *K*-bands (as labelled). KMOS^{3D} probes the underlying population of massive galaxies at $0.7 < z < 2.7$ and $K_{AB} < 23$ mag well, the density distribution shown in grey shades.

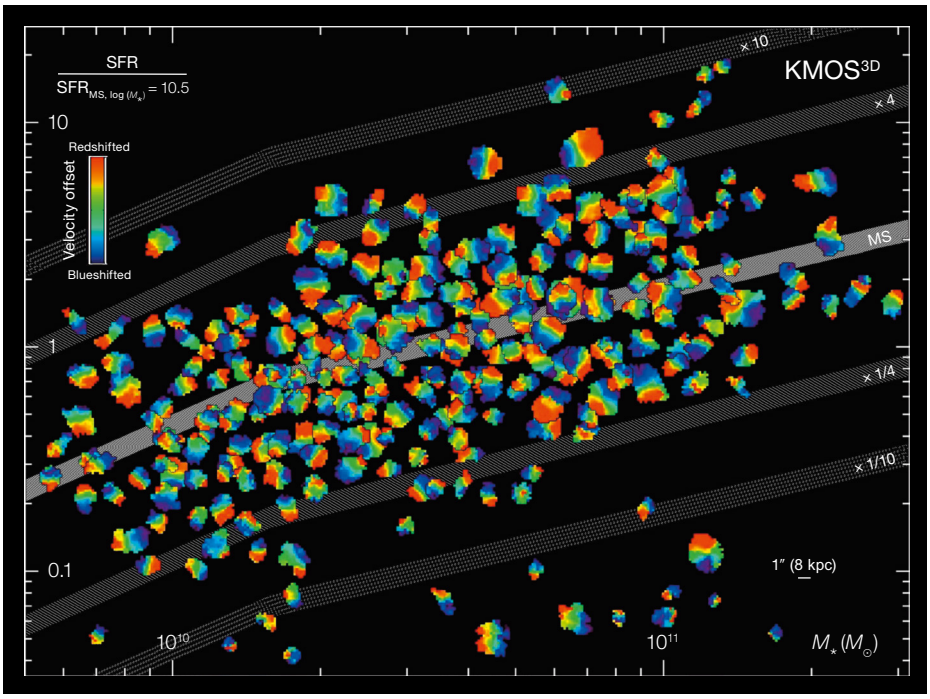

Figure 2. Overview of the Hα velocity fields for 250 resolved and representative KMOS^{3D} galaxies (half at $z \sim 0.9$ and half at $z \sim 2.3$), plotted on the same angular scale and in the same parameter space as in Figiure 1. The monotonic velocity gradients, as well as other characteristic properties of ordered rotation in discs, are identified in the majority of the galaxies, and even among several galaxies well below the MS.

baryon-dominated on scales of ~ 10–15 kpc (Figure 3). Kinematic modelling of 240 well-resolved discs with high S/N data showed that gas and stars dominate the total dynamical mass budget, making up ~ 55% of it on average and reaching ~ 90% at $z \sim 2.3$, leaving little room for dark matter within the disc's half-light radius $R_{1/2}$ at $z > 2$ (Wuyts et al., 2016b). However, the scatter in baryonic mass fractions at fixed redshift is large as a result of correlations with mass surface densities. These effects are reflected in the evolution of the Tully-Fisher relation, connecting the disc circular velocity and mass, from KMOS^{3D} (Übler et al., 2017). A combination of three factors can explain the trends in both the mass budget and the Tully-Fisher relation: the gas and baryonic fractions of the discs increase with look-back time as enhanced cosmic accretion promotes high baryon concentrations at the centre of dark matter halos; these halos have shallow profiles; and more compact discs do not probe as far into their host dark matter halo.

Recent exploration of the outer rotation curves of high-redshift discs led to the exciting discovery of steep declines in velocity beyond a peak at radius $r \sim 1.3\, R_{1/2}$, in stark contrast to the findings at low redshift. In very deep SINFONI observations of six high-mass SFGs probing out to 2–3 times the half-light radius, the slopes are as steep as or steeper than the Keplerian decline ($v_{rot}\, r^{-1/2}$) for a disc purely supported by rotation, and detailed modelling implies dark matter fractions of 20% within

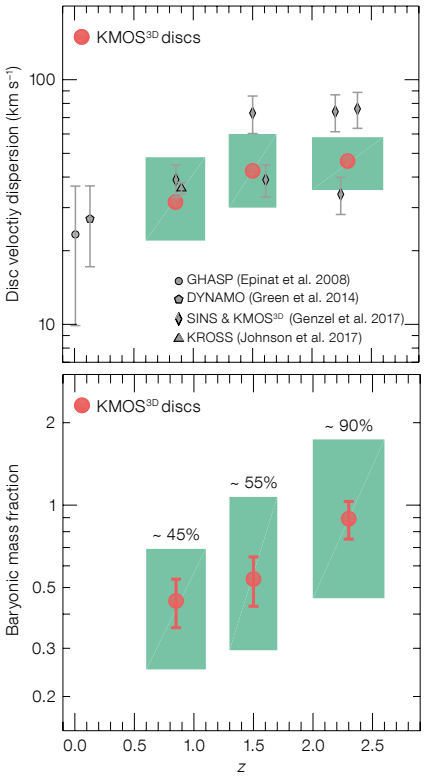

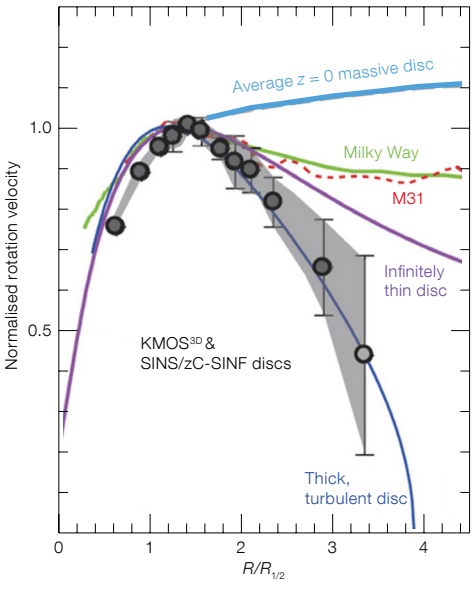

Figure 3. Disc velocity dispersions, baryonic mass fractions on disc scales, and composite rotation curve of $z \sim 0.7$–2.7 discs. In the left panels, median values and 68% percentiles of the distributions for KMOS^{3D} discs in three redshift slices are plotted as red circles and green boxes. In the top left panel, selected results from IFU observations of Hα from other samples, and from individual galaxies with the most detailed constraints, are included (see legend). In the right panel, the effects of the elevated gas turbulence and baryon fraction at high redshift are reflected in the composite rotation curve based on stacked data and individual velocity curves from KMOS^{3D} and the SINS/zC-SINF SINFONI survey (filled circles and grey polygons, respectively). The decline at large radii is steeper than for pure rotation in a disc of similar mass, and is in stark contrast to the much flatter slopes in massive $z \sim 0$ discs, including the Milky Way and M31, that are dominated by dark matter in their outer disc regions (coloured lines).

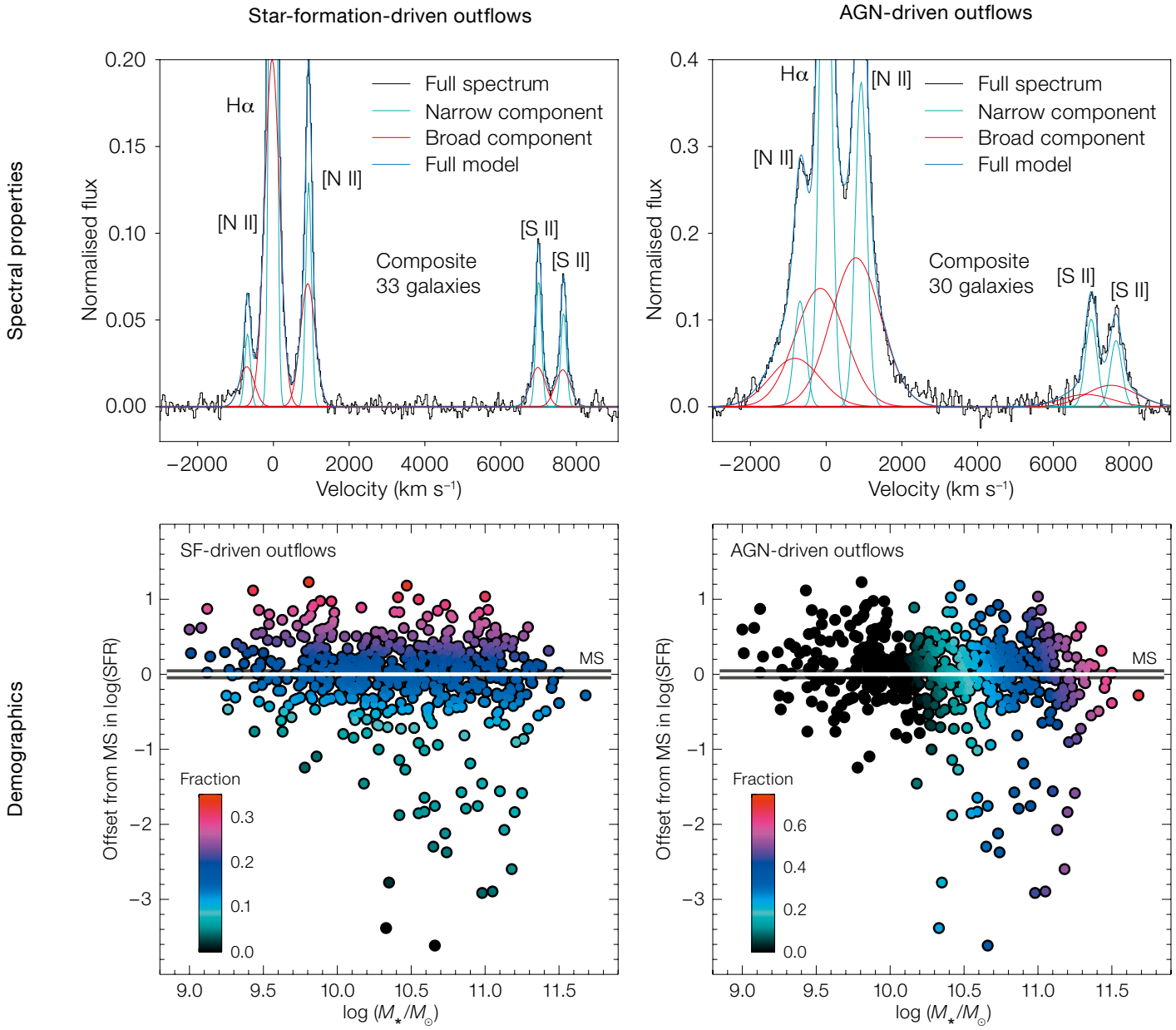

a half-light radius (Genzel et al., 2017). KMOS^{3D} substantiated this breakthrough by showing, through a novel stacking technique, that outer rotation curves declining to 3–4 times $R_{1/2}$ are likely to be a widespread feature of $\log(M_*/M_\odot) \sim 9.5$ star-forming discs around cosmic noon (Lang et al., 2017). In local spiral galaxies, the typically flat rotation curves are the hallmark of dominant dark matter in outer disc regions. At high redshift however, the dominance of baryons within the shallower inner dark matter potential leads to declining rotation curves, with the considerable dynamical support from random motions further steepening the falloff. These results support the lesser role of dark matter on disc scales implied by the mass budget and Tully-Fisher studies, independently of assumptions about the light-to-baryonic-mass conversions. These findings also link massive $z \sim 1$–3 SFGs to their descendants — high-mass early-type galaxies and strongly bulged discs at $z \sim 0$ — which also have low central dark matter fractions.

Figure 4. Distinct spectral properties and demographics of star-formation-driven (left) and AGN-driven (right) galactic-scale winds obtained from ~ 600 galaxies at $0.7 < z < 2.7$ mostly from KMOS^{3D}. The composite spectra (top panels) from the best quality data are plotted with black lines, and the best-fit narrow+broad component emission tracing H II regions and outflows are shown in cyan and orange, respectively. The trends in outflow incidence with stellar mass and offset from the MS at the mass and redshift of each galaxy (bottom panels) are coded according to the colour bars in each panel and sampled at the locations of the individual objects.

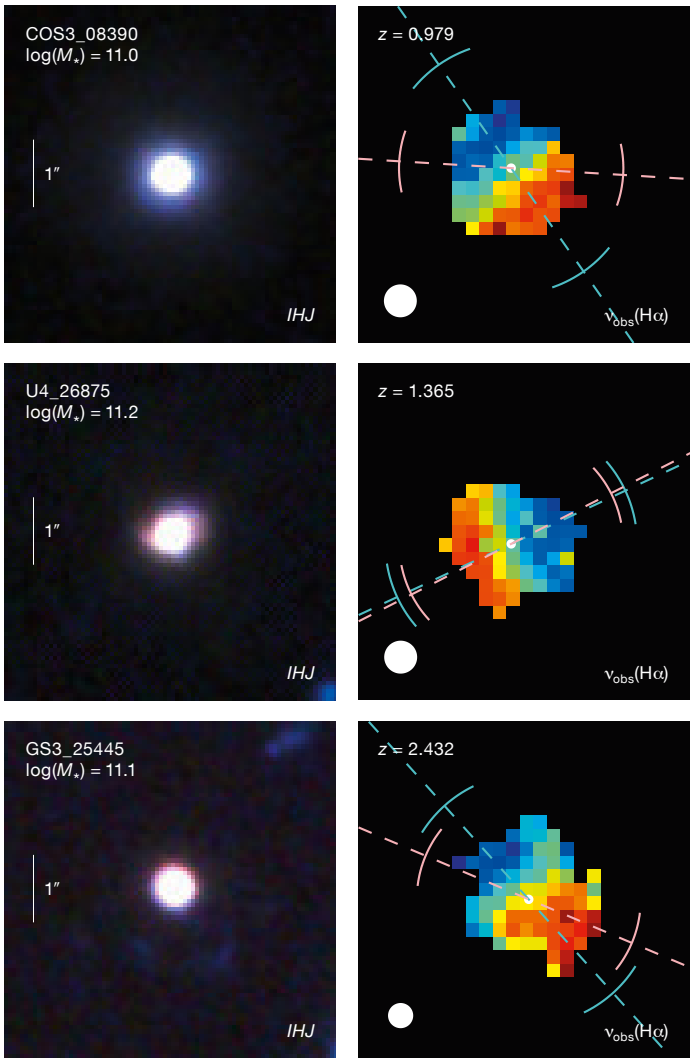

Figure 5. Three examples from among 35 massive compact SFGs observed in KMOS3D. Their HST *IJH*-band morphologies reveal a dominant dense compact stellar component (left panels). KMOS observations of their Hα velocity fields are shown in the right panel; the white circle diameter corresponds to the FWHM of the point spread function of the data. Most of these KMOS observations revealed clear signatures of ordered rotation, supporting the scenario in which they are the immediate progenitors of compact disc-like quiescent galaxies at high redshift.

Demographics and physical properties of galactic outflows

Galactic winds have long been observed in distant SFGs and luminous quasars via high-velocity, blue-shifted absorbing gas detected in galaxy-integrated rest-ultraviolet spectra. In rest-optical nebular line emission, outflows manifest themselves as a broad component lying underneath a narrower component from star formation; their separation is facilitated with IFU data. SINFONI observations of a few tens of objects with ~ 1–2 kpc resolution detected star formation (SF)-driven outflows, characterised by broad emission with FWHM ~ 400–500 km s^{-1}, across the discs. They are typically associated with brighter star-forming clumps, while faster winds (FWHM ~ 1000–2000 km s^{-1}) originate from the nuclear regions in the most massive galaxies hosting an AGN. Analysis of Hα+[N II]+[S II] emission of ~ 600 galaxies spanning $9 < \log(M_*/M_\odot) < 11.7$, mostly from KMOS3D, revealed the distinct demographics and physical properties of outflows (Figure 4, Förster Schreiber et al., 2018; also Genzel et al., 2014). The prevalence of SF-driven outflows depends on star formation properties, with fractions increasing above the MS and reaching up to ~ 40% at SFR surface densities $> 1\ M_\odot\ \mathrm{yr}^{-1}\ \mathrm{kpc}^{-2}$. In contrast, AGN-driven outflows are rare below $\log(M_*/M_\odot) \sim 10.7$ and rapidly become ubiquitous above this mass, being present in ~ 75% of $\log(M_*/M_\odot) > 11.2$ galaxies. Similar to AGN, their incidence depends primarily on stellar mass and its central concentration, but is higher than that of AGN identified by any one diagnostic alone (for example, X-ray properties), thus reflecting the variability of the AGN phenomenon in different tracers. The homogeneous sampling and deep integrations of KMOS3D observations indicate that the incidence trends are not caused by S/N variations across galaxy parameter space. The outflows, along with the elevated disc turbulence, are expected to efficiently redistribute metals within the galaxies, and could explain the typically flat radial metallicity gradients inferred from KMOS3D maps of the diagnostic [N II]/Hα flux ratio (Wuyts et al., 2016a).

The velocities of SF-driven winds vary little with galaxy mass, implying that the relative bulk of expelled gas escapes only from $\log(M_*/M_\odot) \lesssim 10.3$ systems, while more massive galaxies drive so-called "fountains". Surprisingly, the inferred mass outflow rates $\dot{M}_{\mathrm{out}}$ are only ~ 0.1–0.2 times the SFRs at all galaxy masses, at odds with theoretical work that requires mass loading factors $\eta = \dot{M}_{\mathrm{out}}/\mathrm{SFR}$ above unity and $\propto 1/M_*^{0.35-0.80}$ to reproduce the observed slope of the galaxy mass–metallicity and galaxy mass to halo mass relationships at $\log(M_*/M_\odot) < 10.7$. This tension could be alleviated if substantial amounts of mass, momentum, and energy are contained in much hotter and/or colder wind phases than the ~ 10^4 K ionised gas probed by Hα, as inferred in nearby starburst winds.

The faster, high-duty-cycle AGN-driven winds at high masses have mass loading factors comparable to those of the SF-driven winds but carry 10 times as much momentum and 50 times as much energy, so they can escape the galaxies, contribute to heating halo gas, and help prevent further gas infall. Numerical simulations suggest that such a mechanism, which also acts at the modest AGN luminosities and Eddington ratios of the majority of the KMOS3D AGN, may be more effective at widespread and long-term galaxy quenching than ejective QSO-mode feedback in rare, high luminosity, high-Eddington-ratio AGN. The sharp increase in the incidence of AGN-driven outflows near the transition mass above which passive galaxies become prevalent and both galactic molecular gas fractions and specific SFRs drop steeply, strengthens the notion of a

causal link between AGN activity and quenching.

Star-forming discs and rejuvenation in compact galaxies

A strength of the KMOS^{3D} strategy is to allow a systematic exploration of emission line properties in rarer subsets of galaxies, with consistent comparisons to the underlying population. Massive compact SFGs at $z \sim 1$–3 have received much attention in recent years as potential immediate progenitors of dense massive quiescent galaxies. In two-thirds of the 35 compact SFGs observed in KMOS^{3D}, spatially resolved line emission reveals rotating gas discs with up to twice the extent of the compact stellar cores (Figure 5; Wisnioski et al., 2018). Their kinematic properties are similar to those of mass-matched, more extended SFGs in KMOS^{3D}. They host AGN 1.4 times more often, in agreement with other recent studies, and they commonly drive powerful nuclear outflows. The rotation observed in the compact SFGs, and the growing evidence from morphologies and stellar kinematics that high-redshift passive galaxies are disc-like systems, support this evolutionary link.

Pushing into a regime so far unexplored with IFUs at $z > 1$, line emission was also detected in ~ 20% of the KMOS^{3D} targets classified as quiescent based on their rest-frame colours (Belli et al., 2017). Half of them exhibit spectral signatures revealing the persistence of AGN activity and gas outflows well into quenching. In the other sources, the Hα luminosities confirm the low star formation activity with SFR(Hα) ~ 0.2–7 $M_{\odot}$ yr^{-1}, but, surprisingly, their average [N II]/Hα ratio indicates metallicities ~ 3 times lower than in MS SFGs of the same mass, and half also exhibit resolved gas discs. These properties suggest rejuvenation, where the low-level star formation is fuelled by recent accretion of metal-poor gas via cosmic flows or minor mergers rather than being associated with advanced stages of disc fading.

Outlook

The rich scientific outcome of surveys such as KMOS^{3D} and other major campaigns at the VLT underscores the tremendous value of large and coherent observing programmes in advancing our knowledge of galaxy evolution. Comparable efforts in the future with KMOS, other instruments at the VLT, and other facilities such as ALMA and NOEMA will be important to better trace the baryon cycle in and out of galaxies, constrain their stellar composition and kinematics, and systematically explore their cold interstellar medium at all accessible redshifts — paving the way towards the Extremely Large Telescope and James Webb Space Telescope era.

Acknowledgements

We thank the ESO staff on Paranal for excellent and enthusiastic support throughout the five years and numerous runs during which the KMOS^{3D} observations were collected.

References

Belli, S. et al. 2017, ApJ, 841, L6
Burkert, A. et al. 2016, ApJ, 826, 214
Förster Schreiber, N. M. et al. 2011, The Messenger, 145, 39
Förster Schreiber, N. M. et al. 2018, ApJ Suppl., 238, 21
Genzel, R. et al. 2011, ApJ, 733, 101
Genzel, R. et al. 2014, ApJ, 796, 7
Genzel, R. et al. 2017, Nature, 543, 397
Glazebrook, K. 2013, PASA, 30, 56
Krumholz, M. R. et al. 2018, MNRAS, 477, 2716
Lang, P. et al. 2014, ApJ, 788, 11
Lang, P. et al. 2017, ApJ, 840, 92
Momcheva, I. G. et al. 2016, ApJS, 255, 27
Tadaki, K. et al. 2017, ApJ, 834, 135
Übler, H. et al. 2017, ApJ, 842, 121
van der Wel, A. et al. 2014, ApJ, 788, 28
Whitaker, K. E. et al. 2014, ApJ, 795, 104
Wisnioski, E. S. et al. 2015, ApJ, 799, 209
Wisnioski, E. S. et al. 2018, ApJ, 855, 97
Wuyts, E. et al. 2016a, ApJ, 827, 74
Wuyts, S. et al. 2016b, ApJ, 831, 149

VLT colour-composite image of the centre of the starburst galaxy NGC 1313; the filters used are *R*, *B*, *z* and narrow-band Hα, [O I] and [O III].